

the observation of activated transport by Gorbachev *et al.*⁹ in some of their samples. Within the gap the transport mechanism is quantum tunneling, a phenomenon that has no classical analog. Therefore the applicability of the semiclassical Eqs. 1 and 2 to this regime is unclear and a fully quantum mechanical theory of transport is necessary.

A rigorous, fully quantum mechanical approach to calculations of multi-terminal transport coefficients of nanostructures is provided by Büttiker-Landauer theory.¹⁴ However, the conceptual framework of Büttiker-Landauer theory differs from that of the topological arguments⁹ that have been outlined above. For example, within Büttiker-Landauer theory, in the linear response regime (i.e., in the limit where the applied bias voltages and currents approach zero), the four-terminal resistances depend only on the set of quantum electron transmission probabilities $\{T_{i,j}\}$ between all pairs of contacts $\{i,j\}$ and the reflection probabilities $\{R_{i,i}\}$ at contacts $\{i\}$ evaluated at the Fermi energy (or, at finite temperatures, at energies near the Fermi energy). In this limit, the electric field \mathbf{E} that appears in Eq. 2 goes to zero, and therefore in this limit it has no effect on $\{T_{i,j}\}$ and $\{R_{i,i}\}$. Therefore, according to Büttiker-Landauer theory, the topological mechanism of valley currents that is embodied in the term $\mathbf{k} \times \Omega_{\mathbf{k}}$ in Eq. 1 has *no* effect on four-terminal resistances (or more generally on two-, three- or other multi-terminal resistances, including non-local resistances) in the linear response regime. Thus it follows from Büttiker-Landauer theory that non-local resistance measurements in the linear response regime can not provide experimental evidence of topological effects arising from the electric field in Eq. 2.

In other words, Büttiker-Landauer theory shows that non-local (and other) resistances measured in the linear response regime do not depend on whether electrons travel through the sample under the influence of an electric field due to applied bias voltages or simply scatter through the sample freely in the energy window between the highest and lowest contact electrochemical potentials without being subjected to any driving electric field. This means that the effects of the topological term $\mathbf{k} \times \Omega_{\mathbf{k}}$ in Eq. 1 that arise from the driving electric field cannot be detected by local or non-local resistance measurements in the linear response regime.

It is therefore of interest to explore theoretically the multi-terminal resistances and valley currents in fully quantum mechanical models of graphene devices with broken inversion symmetry from the perspective of Büttiker-Landauer theory. This is done in the present paper for transport in graphene nanostructures subjected to staggered potentials in the linear response regime. It will be shown here that the application of a staggered potential results in strong enhancement of the non-local four-terminal resistance when the Fermi level is close to the Dirac point energy, in qualitative agreement with the experimental findings of Gorbachev *et al.*⁹ Despite the studied nanostructures having atomically abrupt boundaries where electrons scatter strongly and crystal momentum is not conserved, valley currents, up to several times larger than the conventional electric current, will be shown to appear in response to electrochemical potential differences between the electrodes when the Fermi level is near the Dirac

point of graphene nanostructures with broken inversion symmetry. These large valley currents are not generated by the topological mechanism embodied in Eqs. 1 and 2 since the present calculations are in the linear response limit where the driving electric field \mathbf{E} in Eq. 2 tends to zero and therefore it does not appear in the Hamiltonian of the system in these Büttiker-Landauer theory-based calculations. Because these strong valley currents occur in a gap in the energy spectrum of the nanostructure they require electron tunneling and consequently their strength decays rapidly as the distance from a contact that injects electrons into the graphene nanostructure increases. These valley currents will be seen to be chiral and to travel along the edge of the graphene that is in contact with an electrode that injects electrons into the graphene. If electrons are injected into the graphene nanostructure with broken inversion symmetry from a scanning tunneling microscope (STM) tip the valley currents will be shown to form a vortex circulating around the location at which the electron injection occurs. At Fermi energies further from the Dirac point and outside of the gap in the density of states of the nanostructure, valley currents are also induced by bias voltages applied to the nanostructure. However in this regime they are found to be weaker, not to require inversion symmetry breaking, and to extend into regions of the nanostructure that are not close to the contacts.

The remainder of this paper is organized as follows. In Section II The model of graphene nanostructures with broken inversion symmetry coupled to current and voltage contacts that is studied in this work is presented. Büttiker-Landauer theory and the Lippmann-Schwinger equation and how they apply to this model are outlined. Valley currents, valley velocity fields and non-local resistances are defined and the methodology used to calculate them is described. The numerical results obtained from these calculations are presented in Section III. The significance of the present findings is discussed in Section IV.

II. MODEL AND FORMALISM

In this paper the graphene nanostructures will be described by the standard nearest neighbor tight-binding Hamiltonian on a honeycomb lattice,

$$H_{\text{GN}} = \sum_n \epsilon_n a_n^\dagger a_n - \sum_{\langle n,m \rangle} t_{nm} (a_n^\dagger a_m + h.c.), \quad (3)$$

where ϵ_n is the on-site energy, $t_{nm} = t = 2.7$ eV defines the matrix element between p_z orbitals on nearest-neighbor atoms and the spin index is suppressed. This Hamiltonian with $\epsilon_n = 0$ is known to describe the π band dispersion of graphene well at low energies,¹⁵ and has been used in numerous studies of electron transport in graphene nanostructures.¹⁶ In order to introduce inversion symmetry breaking into the model, the simple choice $\epsilon_n = \pm\Delta$ is made so that ϵ_n is positive on one atom of the graphene unit cell and negative on the other. The amplitude of the symmetry breaking energy is chosen to be $\Delta = 0.0602$ eV consistent with estimates for graphene on hBN reported in Ref. 11.

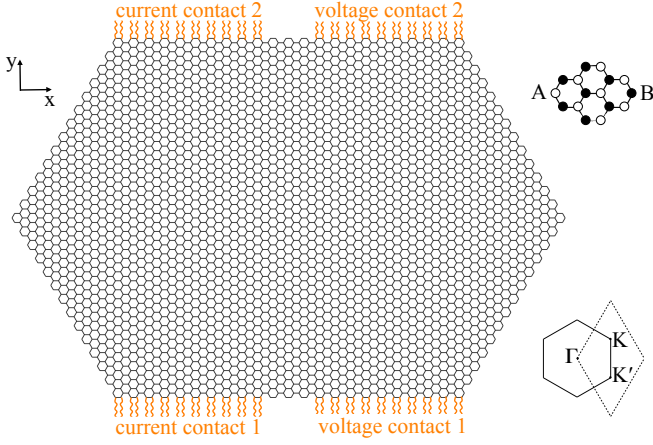


Figure 1. (Color online) Graphene nanostructure with armchair edges. The size of the nanostructure in the y -direction is 9.838 nm. Electron stream is injected through current contact 1 and exits through current contact 2. There is no net electric current entering or leaving through the voltage contacts 1 and 2; the potential difference between them is measured. Wavy lines represent ideal semi-infinite 1D leads connecting graphene C atoms to electron reservoirs. Upper right inset: The graphene sublattices A (B) = open (filled) circles. Lower right inset: Hexagonal (solid) and rhombic (dotted) Brillouin zones of graphene. K and K' are the two Dirac points.

This idealized model has been chosen since the purpose of this paper is to investigate the fundamental effects of inversion symmetry breaking in its simplest form on multi-terminal transport coefficients and valley currents within the fully quantum mechanical Büttiker-Landauer framework. It should be noted that the graphene on hBN system is more involved since the lattice parameters of hBN and graphene have a 2% mismatch and local configurations with N atoms under the centers of graphene hexagons and B atoms under C atoms have the lowest energy.¹¹ However, these complications will not be considered here.

In Büttiker-Landauer theory,¹⁴ at zero temperature and in the linear response regime, the currents I_i flowing towards the nanostructure in contacts i are related to the electrochemical potentials μ_i of the contacts by

$$I_i = \frac{q_e}{h} (N_i \mu_i - \sum_j T_{i,j} \mu_j) \quad (4)$$

where N_i is the number of electronic modes incident on the nanostructure from contact i and $T_{i,j}$ is the multichannel electron transmission probability from contact j to contact i . $T_{i,i} = R_{i,i}$ is the multichannel electron reflection probability from the nanostructure in contact i .

The coefficients $T_{i,j}$ that enter the Büttiker-Landauer theory are calculated in this paper as in many previous theoretical studies of quantum transport in nanostructures^{17–30} with semiconducting,^{19–21,23,29} molecular,^{17–28,30} metallic,^{17–30} magnetic,^{23,25,28,29} and carbon-based²⁸ constituents. Each contact is represented by a set of ideal semi-infinite one-dimensional (1D) tight-binding leads (the wavy lines in Fig. 1) with one orbital per site and nearest neighbor hopping.

One such ideal lead is attached to each peripheral site of the graphene nanostructure that is adjacent to a contact. The Hamiltonian of lead n is

$$H_{Ln} = \sum_r \epsilon_n b_r^\dagger b_r - \sum_{\langle r,s \rangle} t (b_r^\dagger b_s + h.c.), \quad (5)$$

where t is the same as in H_{GN} (Eq. 3). The site energy ϵ_n in Eq. 5 is the same as that of the site of the graphene nanostructure to which the lead is connected. The coupling Hamiltonian between lead n and the edge site of the graphene nanostructure is

$$W_n = -t(b_n^\dagger a_n + h.c.), \quad (6)$$

The quantum transmission amplitudes for an electron to scatter at energy E via the nanostructure from one 1D ideal lead to another are found by solving the Lippmann-Schwinger equation

$$|\psi^m\rangle = |\phi_0^m\rangle + G_0(E)W|\psi^m\rangle, \quad (7)$$

where $|\phi_0^m\rangle$ is an electron eigenstate of the m^{th} ideal semi-infinite lead that is decoupled from the graphene nanostructure, $G_0(E)$ is the Green's function of the decoupled system of the ideal leads and the graphene nanostructure, and $W = \sum_n W_n$ is the coupling between the graphene nanostructure and the ideal leads. $|\psi^m\rangle$ is the scattering eigenstate of the complete coupled system associated with the incident electron state $|\phi_0^m\rangle$. Then

$$T_{i,j}(E) = \sum_{n,m} |t_{nm}^{ij}(E)|^2 v_n^i / v_m^j \quad (8)$$

where $t_{nm}^{ij}(E)$ is the quantum transmission amplitude [obtained from the scattering state $|\psi^m\rangle$ defined by Eq. (7)] for an electron at energy E to scatter via the graphene nanostructure from ideal 1D lead m of contact j to ideal 1D lead n of contact i . The sum is over ideal leads n (m) in contact i (j). $v_{n(m)}^{i(j)}$ is the electron velocity in ideal 1D lead n (m) of contact i (j) at energy E ; $v_n^i = \frac{1}{\hbar} \frac{\partial \epsilon}{\partial k}$ where ϵ are the energy eigenvalues of the Hamiltonian H_{Ln} [Eq. 5] of an infinite ideal 1D tight binding chain.

Having evaluated $T_{i,j}$ at the Fermi energy in this way, the Büttiker equations 4 are solved in the linear response regime to find the non-local 4-terminal resistance

$$R_{NL} = \Delta V / I \quad (9)$$

where I is the current passing through the current contacts and $\Delta V = \Delta \mu / q_e$ is the potential difference between the voltage contacts; see the contacts in Fig. 1.

The valley currents induced in the nanostructure in response to the electrochemical potential differences between the various contacts in the linear response regime are estimated as follows: The scattering state $|\psi^m\rangle$ of electrons injected into the nanostructure from ideal 1D lead m is calculated at the Fermi energy for every lead m by solving the Lippmann-Schwinger equation (7). Then the scattering state $|\psi^m\rangle$ is projected onto the subspaces of Bloch states of graphene that belong to the K and K' valleys. This yields the projected valley

states, $|\psi_K^m\rangle$ and $|\psi_{K'}^m\rangle$, respectively. For this purpose a Bloch state is assigned to the K (K') valley if its wave vector lies within the upper (lower) half of the rhombic Brillouin zone defined by the dotted boundary in the lower right inset of Fig. 1.

The ξ -component of the velocity operator for electrons within the graphene nanostructure is

$$v_\xi = \frac{1}{i\hbar} [\xi, H_{GN}] \quad (10)$$

where $\xi = \sum_p \xi_p a_p^\dagger a_p$ and ξ_p is the ξ -coordinate of atomic site p of the graphene nanostructure. The expectation value of v_ξ in the graphene nanostructure in the state $|\psi^m\rangle$ is then

$$\langle \psi^m | v_\xi | \psi^m \rangle = \frac{it}{2\hbar} \sum_{k,l} (\xi_k - \xi_l) (\psi_k^{m*} \psi_l^m - \psi_k^m \psi_l^{m*}) \quad (11)$$

where k and l are nearest neighbor sites of the graphene nanostructure, $\xi_l = x_l$ or y_l , $\psi_l^m = \langle Z_l | \psi^m \rangle$ and $|Z_l\rangle$ is the $2p_z$ orbital of the carbon atom at site l .

For a graphene nanostructure with multiple contacts i each at its own electrochemical potential μ_i the electron transport through the device is governed by a weighted average over the velocities associated with the scattering states injected by the various ideal leads m_i that make up all of the contacts i . The relevant weighted average will be defined here as

$$v_\xi = \sum_{m,i} \langle \psi^{m_i} | v_\xi | \psi^{m_i} \rangle \Delta\mu_i / \sum_{m,i} \Delta\mu_i \quad (12)$$

where $\Delta\mu_i = \mu_i - \mu_{\min}$ and μ_{\min} is the electrochemical potential of the contact with the lowest electrochemical potential.

The weighted valley velocities $v_{K\xi}$ and $v_{K'\xi}$ for electrons in valleys K and K' are defined similarly by replacing $|\psi^m\rangle$ and $|\psi^{m_i}\rangle$ in Eqs. (11) and (12) by their projections $|\psi_K^m\rangle$ and $|\psi_{K'}^m\rangle$, and $|\psi_K^{m_i}\rangle$ and $|\psi_{K'}^{m_i}\rangle$ onto the valleys K and K' , respectively. The weighted valley velocity is then defined as

$$v_\xi^{\text{val}} = (v_{K\xi} - v_{K'\xi}) \quad (13)$$

Equation (11) expresses the expectation value of the electron velocity as a sum of terms evaluated at pairs (k, l) of nearest neighbor atoms of the graphene nanostructure. This suggests that each such term be interpreted as the value of the velocity field for the scattering state $|\psi^m\rangle$ at the location of each nearest neighbor pair. Assigning this value of the velocity field v_ξ^F arbitrarily to the mid point $(x, y) = ((x_k + x_l)/2, (y_k + y_l)/2)$ of the atomic pair yields

$$\langle \psi^m | v_\xi^F(x, y) | \psi^m \rangle = \frac{it}{\hbar} (\xi_k - \xi_l) (\psi_k^{m*} \psi_l^m - \psi_k^m \psi_l^{m*}) \quad (14)$$

The corresponding velocity field weighted by the contributions of the states contributing to transport through the nanostructure is then, as in Eq. (12), given by

$$v_\xi^F(x, y) = \sum_{m,i} \langle \psi^{m_i} | v_\xi^F(x, y) | \psi^{m_i} \rangle \Delta\mu_i / \sum_{m,i} \Delta\mu_i \quad (15)$$

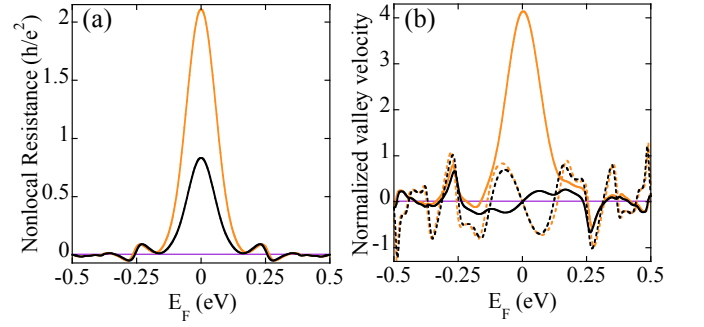


Figure 2. (Color online) Calculated linear response properties vs. Fermi energy of the structure in Fig. 1 at zero temperature. Current I flows through the current contacts with no net current through either voltage contact. Results for symmetry breaking parameter $\Delta = 0.0602$ (0.0) eV are orange (black). (a) Nonlocal resistance R_{NL} [Eq. (9)]. (b) Normalized valley velocities v_x^{val}/v_y and v_y^{val}/v_y [Eq. (12), (13)] are solid and dashed lines, respectively.

Obtaining the weighted velocity fields $v_{K\xi}^F$ and $v_{K'\xi}^F$ for the valleys K and K' similarly by replacing $|\psi^m\rangle$ by the projections $|\psi_K^m\rangle$ and $|\psi_{K'}^m\rangle$, the valley velocity field is defined as

$$v_\xi^{\text{valF}}(x, y) = v_{K\xi}^F(x, y) - v_{K'\xi}^F(x, y) \quad (16)$$

III. RESULTS

The results of Büttiker-Landauer calculations of the non-local four-terminal resistance R_{NL} defined by Eq. (9) for the structure in Fig. 1 at zero temperature in the linear response regime are shown in Fig. 2(a) as a function of the Fermi energy E_F . The Fermi level crosses the Dirac point energy at $E_F = 0$. Near the Dirac point, R_{NL} for the model with $\Delta = 0.0602\text{eV}$ (orange line) exceeds R_{NL} for $\Delta = 0$ (black line) by a factor of ~ 2.5 . Thus within Büttiker-Landauer theory, the breaking of inversion symmetry of the graphene unit cell results in strong enhancement of the non-local resistance near the Dirac point. However, as can also be seen in Fig. 2(a), well away from the Dirac point energy the inversion symmetry breaking has little effect on the non-local resistance.

Since the net electron flow in the structure in Fig. 1 is from current contact 1 to current contact 2 (i.e., in the y -direction), the weighted velocity vector \vec{v} (Eq. 12) is expected to point in the y -direction. Accordingly, v_x in Eq. 12 is found to be zero within numerical error in the present computations. The computed normalized, weighted valley velocities v_x^{val}/v_y and v_y^{val}/v_y are shown in Fig. 2(b). They are found to be non-zero except at isolated values of the Fermi energy both in the presence and absence of symmetry breaking. Note that $v_\xi^{\text{val}}/v_y = I_\xi^{\text{val}}/I$ where I_ξ^{val} is the ξ -component of the valley current and I is the total electric current through the nanostructure. The most striking feature of Fig. 2(b) is the strong peak near the Dirac point ($E_F = 0$) of $v_x^{\text{val}}/v_y = I_x^{\text{val}}/I$ for broken inversion symmetry, (the solid orange curve). At its maximum the valley current in the x -direction exceeds the

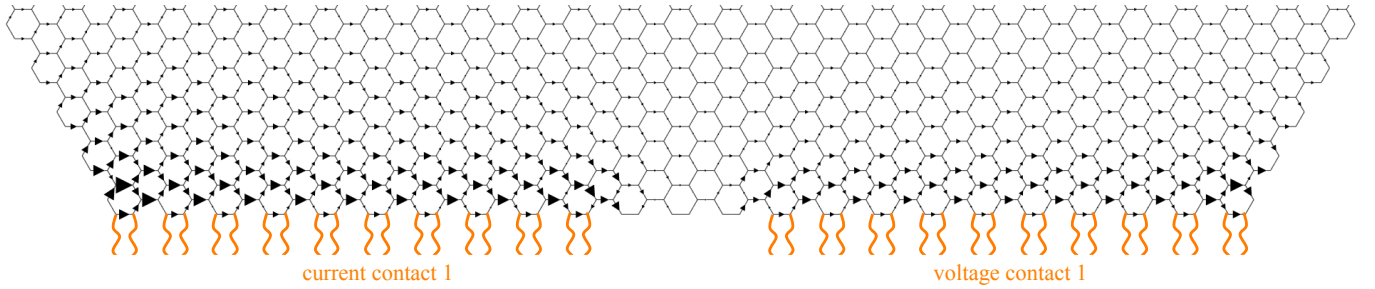


Figure 3. (Color online) Valley velocity field [Eq. (16)] in the lower part of the structure in Fig. 1 for electron flow from current contact 1 to current contact 2 (shown in Fig. 1). For electron flow in this direction, the valley velocity field is much stronger in the vicinity of the contacts shown here than elsewhere in the graphene nanostructure. $\Delta = 0.0602\text{eV}$. $E_F = 0$.

total conventional electric current through the nanostructure by a factor of more than 4. This peak of the valley current is in the gap (of width 0.264 eV) in the energy spectrum of the broken symmetry nanostructure around the Dirac point. By contrast, the x -component of the valley current in the absence of symmetry breaking (solid black curve) and the y -component of the valley current with (orange dashed curve) and without (black dashed curve) symmetry breaking all vanish at the Dirac point and are relatively weak elsewhere. As can also be seen in Fig. 2(b), for E_F well away from the Dirac point energy, both v_x^{val}/v_y and v_y^{val}/v_x are insensitive to the breaking of the inversion symmetry of the graphene.

The full widths of the central peaks of both the non-local resistance and the normalized valley velocity v_x^{val}/v_y for the system with broken inversion symmetry [the orange curves in Figs. 2(a) and (b), respectively] are close in size to the 0.264eV gap in the energy spectrum of the broken symmetry nanostructure. Because the value of the symmetry breaking parameter is relatively small ($\Delta = 0.0602\text{eV}$), the size of the spectral gap is determined mainly by the quantum confinement of the electrons in the graphene nanostructure and the armchair character of the nanostructure's edges.¹⁶ Thus for the same nanostructure but with the symmetry breaking turned off ($\Delta = 0$) the width of the energy gap has a similar value, 0.235 eV. For this reason the main nonlocal resistance peak in Fig. 2(a) has almost the same width for $\Delta = 0$ (the black curve) as for $\Delta = 0.0602\text{eV}$ (the orange curve).

The valley velocity field $\vec{v}^{\text{val}F}(x, y)$ is shown in Fig. 3 for the lower part of the nanostructure in Fig. 1. Inversion symmetry is broken and the Fermi level is at the Dirac point. The valley velocity is large near current contact 1 and voltage contact 1. Its magnitude initially increases but then decreases rapidly with increasing distance from the contacts. The valley velocity is clearly chiral, pointing mainly from left to right near the graphene boundary shown (its overall direction reverses if the sign of Δ , the symmetry breaking parameter, is changed) but it does not extend along the boundary much beyond where a contact ends.

In Fig. 3 the electron flow enters the graphene nanostructure through current contact 1 and exits through current contact 2 that is located outside of the region shown in Fig. 3; see Fig. 1 for its location. If the direction of the electron flow through the graphene nanostructure is reversed, so that elec-

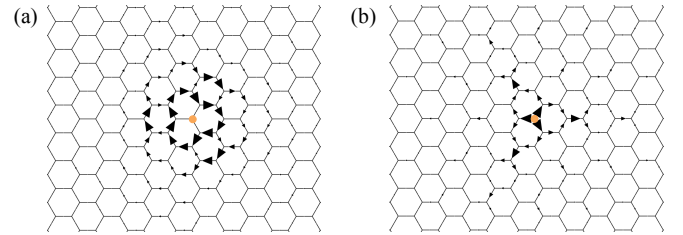


Figure 4. (Color online) (a) Valley velocity field [Eq. (16)] and (b) velocity field [Eq. (15)] for electrons injected into a graphene nanostructure with broken inversion symmetry via a single carbon atom (orange). Only a small part of the graphene nanostructure is shown. $\Delta = 0.0602\text{eV}$. $E_F = 0$.

trons flow instead from current contact 2 to current contact 1 (in Fig. 1), then the valley velocity field becomes strongest near current contact 2 and voltage contact 2, i.e., near the opposite edge of the sample to that where the valley velocity field is strongest in Fig. 3. For electron flow from current contact 2 to current contact 1 the direction of the valley velocity field is from right to left, i.e., its direction is opposite to that in Fig. 3, consistent with the chiral character of the valley current.

The chiral nature of the valley current is further clarified in Fig. 4. Fig. 4 (a) shows the strongest part of the valley velocity field associated with electron injection into a graphene nanostructure with broken inversion symmetry via a single interior carbon atom (colored orange) of the nanostructure, as in an idealized STM setup. The valley velocity field forms a vortex circulating clockwise (counter-clockwise if the sign of Δ is changed) around the injection point, whereas the electron flux travels outwards overall from the injection point as shown in Fig. 4 (b).

In the vicinity of a contact the valley current is due almost entirely to electrons injected into the nanostructure from that contact. This is true even for the voltage contact (Fig. 3) through which no *net* electric current flows since the zero net current is due to equal fluxes of electrons entering and leaving the contact. The valley current of electrons leaving the contact is much larger than that of those entering the contact. Thus a contact through which no net electric current flows can be used to create a valley current into a graphene nanostructure with broken inversion symmetry. I.e., it can in principle

generate a pure valley current.

The results presented above have been for a graphene nanostructure with only armchair edges. Similar calculations for a rectangular structure of similar size (dimensions $9.656\text{nm} \times 9.838\text{nm}$) and similar contacts but with two zigzag and two armchair edges were carried out and yielded qualitatively similar results but the effects of inversion symmetry breaking were found to be much stronger in this case: The non-local resistance for $\Delta = 0.0602\text{eV}$ was found to exceed that for $\Delta = 0$ by more than a factor of 100 for E_F near the Dirac point energy. Also, at its maximum the valley current in the x -direction was found to exceed the total conventional electric current through the nanostructure by a factor of more than 18. These large numbers are attributable to the flat electronic dispersion at graphene zigzag edges³¹ in tight binding models described by the non-interacting electron Hamiltonian, Eq. 3. However, theoretical studies have suggested that electron-electron interactions may give rise to magnetism at zigzag edges.^{32,33} The potential implications of this for valley currents and nonlocal resistances are beyond the scope of the present paper.

Different approaches for realizing valley currents in graphene have also been proposed based on electric fields acting on electrons in the presence of Berry curvature,⁴ graphene point contacts with zigzag edges,³⁴ electron scattering at the boundary between monolayer and bilayer graphene,³⁵ electron scattering at a line defect in graphene,³⁶ illumination of monolayer³⁷ or bilayer³⁸ graphene by circularly polarized radiation, optical injection of a pure valley current in graphene,³⁹ and gate-induced valley filtering in bilayer graphene.⁴⁰ Strong valley current polarizations, comparable to those obtained with the present approach for the structure having both zigzag and armchair edges have been estimated for some of these approaches,^{34,36,38–40} albeit for models of infinite two-dimensional graphene or infinite graphene ribbons. Also, unlike in the present work, the spatial distribution of valley currents was not reported in the previous studies,^{4,34–38,40} and the effects of boundaries between the graphene and source and drain electrodes were not taken into account.

IV. CONCLUSIONS

The present work suggests an approach for creating valley currents in graphene with broken inversion symmetry that dif-

fers fundamentally from previous proposals.^{2,4–9,34–41} As has been explained above, it follows from Büttiker-Landauer theory that in the linear response regime considered here, the transport properties of nanostructures are determined by electron scattering states calculated in the limit where the driving electric field has been sent to zero. Consequently in the linear response regime the acceleration of electrons by the driving electric field has no effect on multi-terminal resistance coefficients or on \bar{I}^{val}/I , the ratio of the valley current \bar{I}^{val} and the conventional electric current I passing through the nanostructure. Thus the valley currents discussed here are not due to electron acceleration in an electric field in the presence of Berry curvature but instead are a direct consequence of non-adiabatic injection of electrons from a contact into the graphene. They are strongest for graphene with broken inversion symmetry in the tunneling regime when the Fermi energy is in the spectral energy gap around the Dirac point. Consequently in this regime these valley currents are strongest close to the graphene/contact boundary. They are chiral and can be very strong close to the Dirac point, i.e., several times larger than the conventional electric current even after averaging over the entire graphene nanostructure. They can appear even at a voltage contact through which no *net* conventional electric current flows provided that electrons are being emitted (and absorbed) by that contact. They are predicted to be realized whenever electrons cross into the graphene at an abrupt boundary (which may be regular or rough on the atomic scale) between a contact and graphene with broken inversion symmetry at energies in the spectral gap around the Dirac point. At Fermi energies well away from the Dirac point (i.e., outside of the gap in the density of states of the nanostructure) valley currents can still be induced by bias voltages applied to the nanostructure but in this regime they are considerably weaker, are not sensitive to whether or not the inversion symmetry of the graphene is broken and are not confined to regions of the nanostructure that are close to contacts. That valley currents can be induced in graphene nanostructures even in the absence of inversion symmetry breaking has been recognized previously,³⁴ and is a consequence of the fact that the Bloch state wave vector need not be a conserved quantity in nanostructures whose translational crystal symmetries are broken due to the presence of boundaries.

This research was supported by NSERC, CIFAR, Westgrid, and Compute Canada.

¹ P. R. Wallace, Phys. Rev. **71**, 622 (1947).

² For a pedagogical review of the Berry phase and related topics see D. Xiao, M.-C. Meng, Q. Niu, Rev. Mod. Phys. **82**, 1959 (2010).

³ T. Ando, T. Nakanishi, R. Saito, J. Phys. Soc. Jpn. **67**, 2857 (1998).

⁴ D. Xiao, W. Yao, Q. Niu, Phys. Rev. Lett. **99**, 236809 (2007).

⁵ R. Karplus and J. M. Luttinger, Phys. Rev. **95**, 1154 (1954).

⁶ M. C. Chang and Q. Niu, Phys. Rev. Lett. **75**, 1348 (1995).

⁷ M. C. Chang and Q. Niu, Phys. Rev. B **53**, 7010 (1996).

⁸ Y. D. Chong, Phys. Rev. B **81**, 052303 (2010).

⁹ R. V. Gorbachev, J. C. W. Song, G. L. Yu, A. V. Kretinin, F. Withers, Y. Cao, A. Mishchenko, I. V. Grigorieva, K. S. Novoselov, L. S. Levitov, A.

K. Geim, Science **346**, 448 (2014).

¹⁰ G. Giovannetti, P. A. Khomyakov, G. Brocks, P. J. Kelly, J. van den Brink, Phys. Rev. B **76**, 073103 (2007).

¹¹ B. Sachs, T. O. Wehling, M. I. Katsnelson, A. I. Lichtenstein, Phys. Rev. B **84**, 195414 (2011).

¹² M. Kindermann, B. Uchoa, D. L. Miller, Phys. Rev. B **86**, 115415 (2012).

¹³ J. C. W. Song, P. Samutpraphoot, L. S. Levitov, arXiv:1404.4019 [cond-mat.mes-hall]

¹⁴ M. Büttiker, Phys. Rev. Lett. **57**, 1761 (1986)

¹⁵ S. Reich, J. Maultzsch, C. Thomsen, and P. Ordejón, Phys. Rev. B **66**, 035412 (2002).

- ¹⁶ For a review see G. Kirczenow and S. Ihnatsenka, Ch. 13 in *Graphene Nanoelectronics: Metrology, Synthesis, Properties and Applications* edited by H. Raza (Springer, Heidelberg, Dordrecht, London, New York, 2012).
- ¹⁷ H. Dagleish and G. Kirczenow, Phys. Rev. B **72**, 155429 (2005); Nano Lett. **6**, 1274 (2006); Phys. Rev. B **73**, 245431, (2006); Phys. Rev. B **73**, 235436, (2006).
- ¹⁸ J. Buker and G. Kirczenow, Phys. Rev. B **72**, 205338, (2005); Phys. Rev. B **78**, 125107(2008).
- ¹⁹ G. Kirczenow, P. G. Piva, and R. A. Wolkow, Phys. Rev. B **72**, 245306 (2005); **80**, 035309 (2009).
- ²⁰ G. Kirczenow, Phys. Rev. B **75**, 045428 (2007).
- ²¹ P. G. Piva, R. A. Wolkow, and G. Kirczenow, Phys. Rev. Lett. **101**, 106801 (2008).
- ²² D. M. Cardamone and G. Kirczenow, Phys. Rev. B **77**, 165403 (2008); Nano Lett. **10**, 1158 (2010).
- ²³ G. Kirczenow, in *The Oxford Handbook of Nanoscience and Technology, Volume I: Basic Aspects*, edited by A. V. Narlikar and Y. Y. Fu, Chap. 4 (Oxford University Press, Oxford, 2010).
- ²⁴ F. Demir and G. Kirczenow, J. Chem. Phys. **134**, 121103 (2011).
- ²⁵ F. Rostamzadeh Renani and G. Kirczenow, Phys. Rev. B **84**, 180408(R) (2011); Phys. Rev. B **85**, 245415 (2012); **87**, 121403 (2013).
- ²⁶ F. Demir and G. Kirczenow, J. Chem. Phys. **136**, 014703 (2012).
- ²⁷ F. Demir and G. Kirczenow, J. Chem. Phys. **137**, 094703 (2012).
- ²⁸ A. Saffarzadeh and G. Kirczenow, Appl. Phys. Lett. **102**, 173101 (2013).
- ²⁹ S. Majumder, B. Kardasz, G. Kirczenow, A. SpringThorpe and K. L. Kavanagh, Semicond. Sci. Technol. **28**, 035003 (2013).
- ³⁰ A. Saffarzadeh, F. Demir, and G. Kirczenow, Phys. Rev. B **89**, 045431 (2014).
- ³¹ K. Nakada, M. Fujita, G. Dresselhaus and M. S. Dresselhaus, Phys. Rev. B **54**, 17954 (1996).
- ³² M. Fujita, K. Wakabayashi, K. Nakada, K. Kusakabe, J. Phys. Soc. Jpn. **65**, 1920 (1996).
- ³³ For a recent review and further references see J. L. Lado, N. García-Martínez, J. Fernández-Rossier, arXiv:1502.07112 [cond-mat.mes-hall]
- ³⁴ A. Rycerz, J. Tworzydło, C. W. J. Beenakker, Nat. Phys. **3**, 172 (2007).
- ³⁵ T. Nakanishi, M. Koshino and T. Ando, Phys. Rev. B **82**, 125428 (2010).
- ³⁶ D. Gunlycke and C. T. White, Phys. Rev. Lett. **106**, 136806 (2011).
- ³⁷ T. Oka and H. Aoki, Phys. Rev. B **79**, 081406(R) (2009).
- ³⁸ D. S. L. Abergel and T. Chakraborty Appl. Phys. Lett. **95**, 062107 (2009).
- ³⁹ L. E. Golub, S. A. Tarasenko, M. V. Entin and L. I. Magarill, Rev. B **84**, 195408 (2011).
- ⁴⁰ D. R. da Costa, A. Chaves, S. H. R. Sena, G. A. Farias and F. M. Peeters Phys. Rev. B **92**, 045417 (2015).
- ⁴¹ W. Yao, D. Xiao, and Q. Niu, Phys. Rev. B **77**, 235406 (2008).